KSME

Springer

Journal of Mechanical Science and Technology 38 (3) 2024

Original Article
DOI 10.1007/s12206-024-0220-z

Keywords:
· Molecular dynamics simulation
· Contact angles
· 1,2-dichloroethane (DCE)
· Oil droplet
· Static behavior of droplet

Correspondence to:
Tae Woo Kwon
twkwon@pusan.ac.kr;
Man Yeong Ha
myha@pusan.ac.kr

Citation:
Kang, Y. J., Kwon, T. W., Ha, M. Y. (2024). Investigation of the behavior of water and oil droplets on nanostructured surfaces: a molecular dynamics simulation study. Journal of Mechanical Science and Technology 38 (3) (2024) 1249~1257. http://doi.org/10.1007/s12206-024-0220-z

Received May 17th, 2023
Revised October 12th, 2023
Accepted November 28th, 2023

† Recommended by Editor Han Seo Ko

Investigation of the behavior of water and oil droplets on nanostructured surfaces: a molecular dynamics simulation study

Yun Ji Kang[1], Tae Woo Kwon[2] and Man Yeong Ha[1]

[1]School of Mechanical Engineering, Pusan National University, 2 Busandaehak-ro 63beon-gil, Geumjeong-gu, Busan 46241, Korea, [2]Rolls-Royce and Pusan National University Technology Centre in Thermal Management, Pusan National University, 2 Busandaehak-ro 63beon-gil, Geumjeong-gu, Busan 46241, Korea

Abstract This study conducted molecular dynamics simulations to estimate the behavior of water and oil droplets on the same surface and to investigate how oil droplets respond to varying surface conditions. The surfaces were considered from a flat plate to pillared surfaces with varying heights. Additionally, three surface conditions were examined by altering the solid-surface characteristic energy: lipophobic (weakly hydrophobic), weak lipophobic, and lipophilic conditions. The results showed that as the pillar height increased, the contact angle of the water droplet on the weak hydrophobic surfaces increased, while that of the 1, 2-dichloroethane (DCE) droplet remained relatively constant. In the case of weak lipophobic conditions, the top and bottom parts of the DCE droplet exhibited distinct behaviors as the pillar height increased. Furthermore, under lipophilic conditions, the oil droplets displayed varying patterns in their shape changes with increasing pillar height. These findings imply that droplet behavior on surfaces can be manipulated by engineering structures without necessitating additional external forces or energy inputs. This research provides valuable insights into the potential for separating and merging different types of liquids.

1. Introduction

The lotus effect, a well-known phenomenon, describes the repulsion of water by lotus leaves. This phenomenon is attributed to the countless nanosized textures on lotus leaves, which prevent water from permeating the surface and promote the formation of water droplets [1]. Similar nanosized protrusions can also be found on the wings of butterflies and the antennae of insects, which enable water repellency and the formation of droplets without wetting the surface. Biomimetic technologies that mimic the hydrophobicity of lotus leaves have been applied in various devices and products, such as advanced smart displays, functional optical films, and automotive glass [2]. Extensive experimental and numerical studies have been conducted to comprehend and apply this surface hydrophobicity in various fields [3-6].

Apart from water, the behavior of oil on surfaces in nature has also been a subject of study. Research has been carried out to understand the lipophobicity of surfaces, aiming to comprehend oil-solid surface interactions and compare them with water-solid surface interactions. Lipophobicity-based techniques have gained significant attention because of their potential effectiveness in oil extraction and recovery. Especially, given the presence of oil on surfaces like rocks, research and development efforts have been devoted to recovering oil by leveraging surface characteristics. Consequently, numerous studies have explored the surface characteristics of oil to optimize oil-recovery efficiency [7-10].

Ji et al. [7] conducted molecular dynamics simulations to investigate the adsorption behavior of heavy oil droplets on silica surfaces with varying hydrophobicity properties. Their findings indicated that fully hydrophobic surfaces create a favorable environment for the interaction of active oil molecules, resulting in the rapid absorption of oil droplets. Guo et al. [8] analyzed the

behavior of water droplets on slippery liquid-infused porous surfaces with hexane between the nanostructures. They observed that the behavior of the hexane layer and the water droplet depended on the thickness of the hexane layer and the characteristics of the nanostructures. Gao et al. [9] fabricated nanostructures on a surface and studied the behavior of oil droplets in three-phase (oil-air-solid) and four-phase (oil-air-solid-water) systems. They considered different droplet states and multiphase systems and found that the behavior of oil droplets varied depending on these factors. Finally, Xu et al. [10] employed molecular dynamics simulations to estimate the dynamic characteristics of oil droplets on charged surfaces in a three-phase system consisting of water, oil, and rock. Their findings revealed that the surface charge strongly influences the contact angle of oil droplets, resulting in a transition from an oil-wet to a water-wet state as the surface charge changes from negative to positive.

The objective of this study is to estimate the behavior of oil droplets on a nanostructured surface with square pillars using molecular dynamics simulations. The behavior of oil droplets was compared with that of water droplets under the same conditions. Furthermore, we examine various conditions for oil droplets, including different solid-surface characteristic energies, lipophobic, weak lipophobic, and lipophilic conditions. Additionally, the height of the square pillars was also adjusted to study the droplet behaviors. The analysis involved assessing changes in droplet shape and calculating contact angles for comparison purposes.

2. Numerical methodology

2.1 Molecular dynamics simulation

This study conducted molecular dynamics simulations to estimate the behaviors of water and oil droplets on a nanostructured surface with square pillars. Molecular dynamics simulations enable the prediction and estimation of atomic and molecular movements by calculating interatomic potentials. It is useful tool to investigate the phenomena at the nanoscale such as the behaviors of nano-sized droplets [3-5], vaporization under extreme conditions [11], and multi-scale approaches [12].

The open-source software LAMMPS [13] was employed to perform molecular dynamics simulations. For molecular modeling and potential calculations, the CHARMM force field was selected. The interatomic potential function used in this study was described using the Lennard–Jones (LJ) potential, which effectively captures the interactions between atoms or molecules within the system.

The potential energy function on molecules was expressed using the following interatomic potential [13]:

$$U_{total} = U_{bond} + U_{angle} + U_{dihedral} + U_{coulomb} + U_{LJ}. \quad (1)$$

Here, U_{total} represents the summation of the potentials between the atoms and molecules; U_{bond}, U_{angle}, and $U_{dihedral}$ represent the potentials of the tensile force acting between two atoms, the bending between three atoms, and the interatomic torsion among four atoms, respectively. These three potentials act between and among atoms present in the same molecule. Conversely, the other potentials, $U_{coulomb}$ and U_{LJ}, in Eq. (1) represent the potentials acting between a pair of atoms in different molecules. $U_{coulomb}$ describes the Coulomb potential of the electrical force, and U_{LJ} represents LJ potential of van der Waals interaction. As the surface in this study was electrically neutral, the Coulomb potential was not taken into account. Therefore, only the LJ potential was considered between the droplet molecules and the surface atoms. The LJ potential is expressed as follows:

$$U_{LJ} = 4\varepsilon_{ij}\left[\left(\frac{\sigma_{ij}}{r_{ij}}\right)^{12} - \left(\frac{\sigma_{ij}}{r_{ij}}\right)^{6}\right] \quad (2)$$

where ε_{ij}, σ_{ij}, and r_{ij} represent the characteristic energy, characteristic length, and distance between a pair of atoms i and j, respectively. The characteristic energy and length can be calculated using the Lorentz–Bertholet mixing rule [14].

2.2 Computational details

Fig. 1 shows the molecular structures of water and oil, as well as the solid atom structure used in this study. For the water molecule, we used the "transferable intermolecular potential 3 points" (TIP3P) model implemented in the CHARMM force field since it is suitable for a standard state with the pressure of 1 atm and the temperature of 300 K [15, 16]. The TIP3P model uses three sites to represent the three atoms in the water molecule and considers non-bonded interactions, as shown in Fig. 1(a).

Since oil molecules have a macromolecular structure in which numerous molecules are bonded, the molecular weight is significant, and the molecular structure is quite complicated. Moreover, these multiply bonded molecular structures increase the difficulty associated with the simulation of the behaviors of the oil droplet. Thus, in this study, 1, 2-dichloroethane (DCE; $C_2H_4Cl_2$) was used for the oil molecule because of its relatively simple structure [17], as shown in Fig. 1(b). One carbon atom and two hydrogen atoms were combined and assumed as one atom of CH2. Thereafter, the simplified DCE molecule had two CH2 and two chlorines. Table 1 shows the detailed parameters of the water and DCE models for the calculation of the poten-

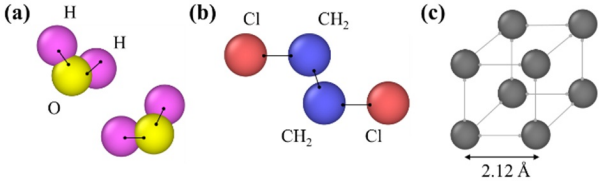

Fig. 1. The molecular structures of (a) water; (b) oil; (c) the solid atom.

Table 1. The detail parameters of water and DCE models.

LJ/Columb				Bond		
Atom	ε [kcal/mol]	σ [Å]	q [e]	Atom	K_{bond} [kcal/mol Å^2]	r_0 [Å]
H	0	0	0.415	H-O	450	0.9572
O	0.102	3.188	-0.830	Cl-CH2	232	1.787
CH2	0.144	3.980	0.227	CH2-CH2	310	1.530
Cl	2.090	3.785	-0.227			

Angle			Dihedral				
Atom	K_{angle} [kcal/mol]	θ [°]	Atom	A1	A2	A3	A4
H-O-H	55	104.52	Cl-CH2-CH2-Cl	1.59	-4.96	0.10	6.46
Cl-CH2-CH2	44	108.02					

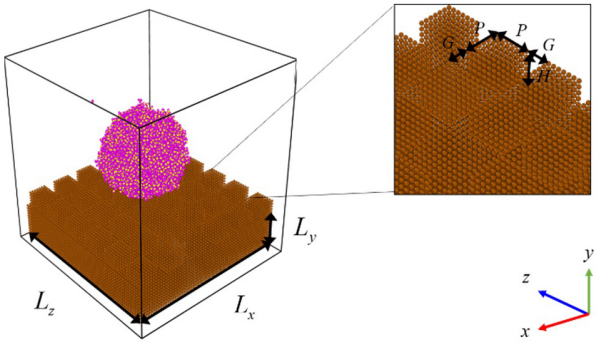

Fig. 2. The computational domain and the initial state of the simulation.

tials in Eq. (1).

Fig. 1(c) shows the structure of the solid atom considered in this study. The hypothetical atoms were assigned to the considered surfaces to exclude the effect of the atom structure. The hypothetical atoms were constructed with a simple cubic structure having a minimum spacing (l_0) of 2.12 Å. To change the surface characteristics of the water and DCE droplets, the characteristic energy of the surface (ε_s) was controlled and employed in the calculation of the LJ potential.

Fig. 2 shows the computational domain and the initial state of the simulation. The solid surface was composed of a flat plate as well as square-pillared structures. The width and depths of the flat plate ($L_x \times L_z$) were 125 Å × 125 Å, and the height of the flat plate (L_y) was 23.3 Å. The square pillar was designed as a square column with a width (P) of 14.7 Å. The gap between the pillars (G) was fixed at 7.33 Å. The height of square pillar (H) varied from 0 to 16.96 Å by a unit of 2.12 Å, which is the minimum spacing in the solid atom structure. The number of solid atoms constituting the surface varied from 43200 to 57312, as the pillar height increased.

To realize the initial spherical shape of the droplets, as shown in Fig. 2, a pre-simulation was performed with only water or DCE molecules. First, 3921 water molecules or 1728 DCE molecules were randomly located in a cube with a dimension of 50 Å × 50 Å × 50 Å. Afterward, the molecules were assembled by interactions during the simulation, and they assumed a spherical shape at equilibrium. Finally, the spherical droplet was set on the surface, as shown in Fig. 2.

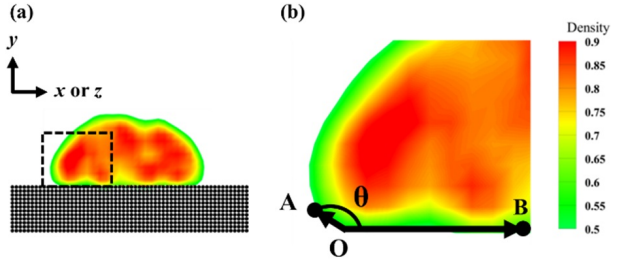

Fig. 3. (a) Normalized density field of droplet; (b) the definition of the contact angle.

Periodic boundary conditions were implemented in the computational domain along x, y, and z directions. Based on the canonical NVT ensemble, the number of atoms (N) and the volume of the computational domain (V) were fixed during the simulation. In addition, the temperature (T) of the domain was fixed at 300 K. In these simulations, the cutoff distance was selected as 12.0 Å.

The time steps were set differently, corresponding to the kinds of molecules and the progress of the simulation. For the water molecules, the time step was selected as 1.0 fs throughout the simulation. Conversely, considering the strong interactions between the DCE molecules, the time step for the DCE molecules was selected as 0.01 fs during the first 0.5 ns to stabilize the simulation. After the first 0.5 ns, it was changed to 1.0 fs, which was the same as that for the water molecules.

To realize the bond and angle potentials used when performing the calculation, the SHAKE algorithm was employed [18]. Wall conditions were applied to solid atoms to exclude their vibration and heat transfer. To integrate the differential equations for the potentials, LAMMPS was used [19-21].

2.3 Contact angle

The contact angles of the water and DCE droplets were defined and measured by the following method. First, the density fields of the water and DCE droplets were derived on the $x-y$ and $z-y$ planes. Furthermore, the density field was normalized by the maximum density value so that the values were between 0 and 1, as shown in Fig. 3(a). Subsequently, the droplet's shape was determined based on a curve that corresponds to a normalized density of 0.5. Fig. 3(b) shows the detailed definition of the contact angle. Point O is defined as the point at which the boundaries of the droplet and the solid surface contact. Point A is a point at the boundary of the droplet, and point B is a point at the center of the droplet–solid interface. Thus, vectors $\overrightarrow{OA}$ and $\overrightarrow{OB}$ represent the tangential vector on the droplet and the vector directing to the center of the droplet–solid interface, respectively. Finally, the angle between these two vectors, θ, is defined as the contact angle,

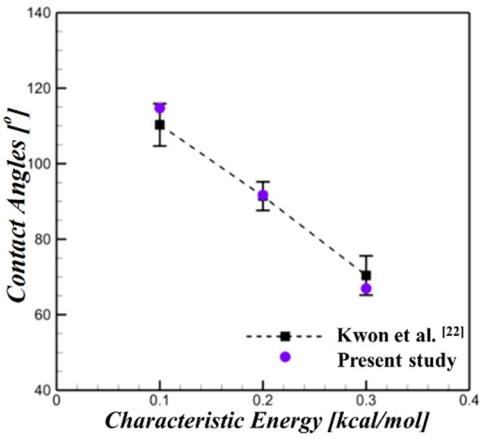

Fig. 4. Comparison of contact angles obtained from this study with Kwon et al. [22].

as shown in Fig. 3(b).

Since the droplet's shape was asymmetric, contact angles were obtained at a total of four positions: two in the $+x$ and $-x$ directions on the $x-y$ plane and two in the $+z$ and $-z$ directions on the $z-y$ plane. The measured four contact angles were averaged. In addition, the time-averaged contact angle was calculated during the final 0.5 ns at the equilibrium state to minimize the effect of the fluctuation of the droplet's shape. The fluctuation of the contact angle is shown in the figures using error bars.

Fig. 4 shows a comparison of the contact angles of the water droplets obtained in this study and those reported from Kwon et al. [22]. The water droplets were located on a flat surface with solid characteristic energies in the range of 0.1–0.3 kcal/mol. In this study, the contact angles were measured as 114.7°, 91.9°, and 68.7° with the solid-surface characteristic energy of 0.1, 0.2, and 0.3 kcal/mol. These values were within the range of the results' fluctuation in the previous study. The comparison of the results verified the simulation method.

3. Results and discussion

3.1 Water and DCE droplets

At first, at the solid characteristic energy of 0.2 kcal/mol, the water and DCE droplets were considered. To study the behaviors of the water and DCE droplets, molecular dynamics simulations were conducted. Based on the validation results at the surface characteristic energy of 0.2 kcal/mol, the water droplet had a contact angle of 91.9°, indicating weak hydrophobicity, and the droplet exhibited a hemispherical shape. Conversely, the DCE droplet exhibited considerably weak interactions with the surface at the solid-surface characteristic energy of 0.2 kcal/mol, resulting in an almost perfect spherical shape. The contact angle of the DCE droplet was 147.91°, demonstrating the lipophobic properties of the surface.

Fig. 5 shows snapshots of the water and DCE droplets at various pillar heights on the solid surface at a solid characteristic energy of 0.2 kcal/mol. Specifically, Figs. 5(a)-(d) show the shapes of the water droplets at pillar heights ranging from 0 to 2.12 Å, 10.60 Å, and 16.96 Å, respectively. As the pillar height increased, more water molecules penetrated the gaps between the pillars, causing water droplets to reach the Wenzel state. Therefore, the water droplet changed from a hemisphere to a near-sphere, as shown in Figs. 5(a)-(d).

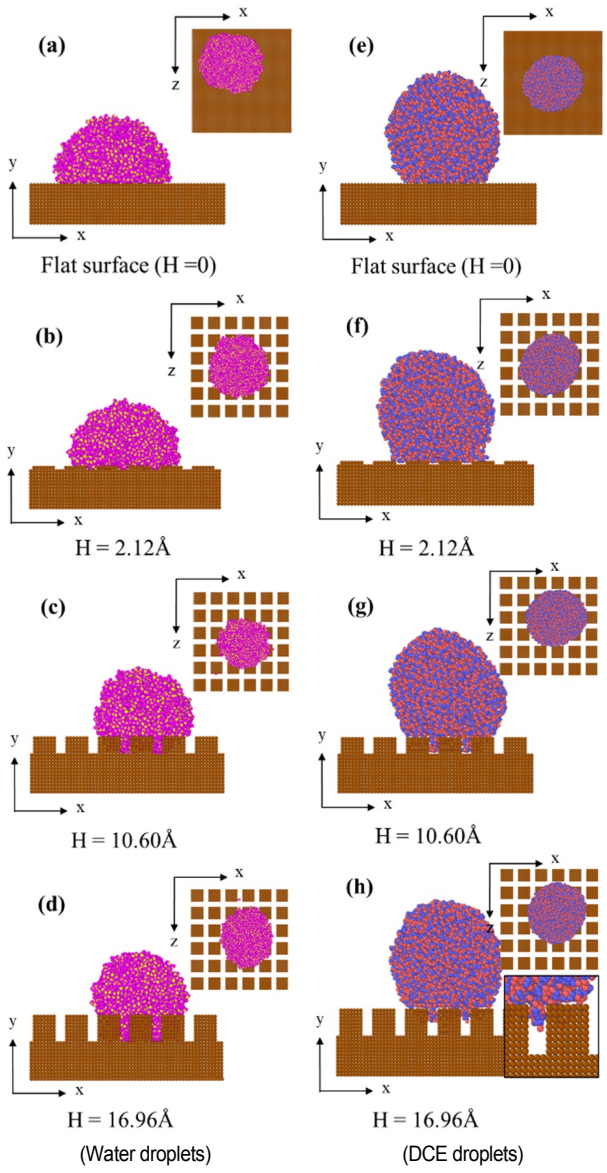

Fig. 5. Snapshots of water: (a)-(d) and DCE; (e)-(h) droplets for different pillar heights at the solid surface characteristic energy of 0.2 kcal/mol.

Figs. 5(e)-(h) show the shapes of the DCE droplets relative to the pillar height at the solid-surface characteristic energy of 0.2 kcal/mol. The DCE droplet exhibited a nearly spherical shape and maintained its shape as the pillar height increased. The intermolecular attraction in DCE was stronger than that in water because of its higher molecular weight. Thus, the intermolecular attraction in DCE dominated the droplet's shape, whereas that in water did not. Therefore, at the solid-surface

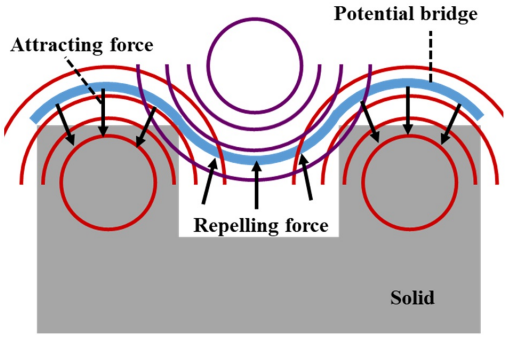

Fig. 6. A potential bridge due to geometrical potentials [23, 24].

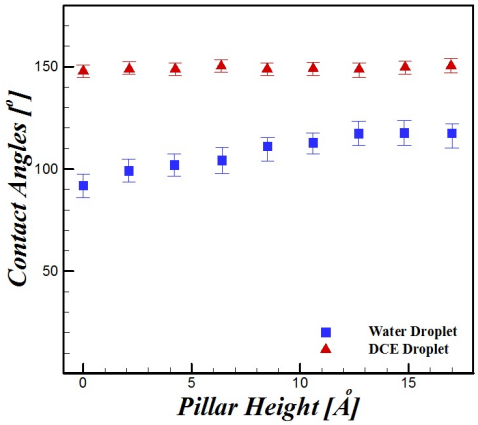

Fig. 7. Contact angles of water and DCE droplets according to the pillar height at the solid surface characteristic energy of 0.2 kcal/mol.

characteristic energy of 0.2 kcal/mol, the DCE droplet formed a spherical shape in the Cassie–Baxter state, regardless of the pillar height.

In the detail view of Fig. 5(h), the DCE molecules penetrated about half of the pillar height, although the DCE droplet was in the Cassie-Baxter state. The DCE molecules penetrated the gaps only about 8.48 Å, not fully because of a potential bridge which is determined by the balance of gravity, attracting force and repelling force [23, 24], as shown in Fig. 6. The DCE droplet on the surface with the solid-surface characteristic energy of 0.2 kcal/mol seems to make a potential bridge at the depth about 8.48 Å from the top of the pillars.

Fig. 7 shows the contact angle of the water and DCE droplets corresponding to the pillar height at the solid-surface characteristic energy of 0.2 kcal/mol. The blue square and red triangle symbols represent the contact angles of the water and DCE droplets, respectively. For the water droplet, as the pillar height increased from 0 to 12.72 Å, the contact angle gradually increased from 91.93° to 98.97°, 101.90°, 104.19°, 111.01°, 112.85°, and 117.22°, resulting in a change in the droplet shape, as shown in Figs. 5(a)-(d). When the pillar height exceeded 12.72 Å, the interaction between the water droplet and the solid surface weakened because of the increased distance from the flat plate. Consequently, at pillar heights over 12.72 Å, no significant effect on the behavior of the water droplet was observed. Thus, at the solid-surface characteristic energy of 0.2 kcal/mol, the hydrophobicity of the surface increased and converged as the pillar height increased.

For the DCE droplet, at the solid-surface characteristic energy of 0.2 kcal/mol, the contact angle remained constant as the pillar height increased. The DCE droplet exhibited contact angles of approximately 147.91 ± 2.53° at all pillar heights, indicating the significant lipophobicity of the surface. The relatively strong intermolecular attractions in DCE, attributed to its large molecular weight, caused the DCE molecules to be more clustered than the water molecules, resulting in a spherical shape. Thus, the large intermolecular attractions in DCE maintained the DCE droplet shape.

At the solid-surface characteristic energy of 0.2 kcal/mol, the water and DCE droplets exhibited different shapes on the same surface.

3.2 DCE droplets on various surfaces

This study investigated the behaviors of the DCE droplets on various surfaces. To implement a weak lipophobic surface or a lipophilic surface, the solid-surface characteristic energy of the surface was changed to 1.0 kcal/mol and 20.0 kcal/mol.

At the solid-surface energy of 1.0 kcal/mol, the DCE droplet on the flat plate had an instinct contact angle of 91.7°, indicating a weak lipophobic surface, similar to that of the water droplet at the solid-surface characteristic energy of 0.2 kcal/mol. On the other hand, the solid-surface characteristic energy of 20.0 kcal/mol indicated the lipophilic characteristics for the DCE droplet. The DCE droplets exhibited a contact angle of 62.31° on the surface with a solid characteristic energy of 20.0 kcal/mol, which shows a lipophilic surface.

Fig. 8 shows snapshots of the DCE droplets at the solid-surface characteristic energy of 1.0 kcal/mol. Figs. 8(a)-(c) show snapshots of the DCE droplets corresponding to the pillar height, while Figs. 8(d)-(f) show schematic diagrams of the droplet shapes. Fig. 8(a) shows the shape of the DCE droplet formed on the flat plate (H = 0). The DCE droplet on the flat plate exhibited a hemispherical shape on the cylinder, as simplified in Fig. 8(d). The top part of the DCE droplet was hemispherical because of the intermolecular attraction in DCE. Conversely, the bottom part of the droplet interacted with the flat plate, resulting in a cylindrical shape.

Fig. 8(b) shows the shape of the DCE droplet at the pillar height of 8.48 Å when the solid-surface characteristic energy was 1.0 kcal/mol. The top part of the DCE droplet almost maintained its shape. However, the bottom part of the DCE droplet permeated the gaps between the pillars and spread on the surface. The contact area between the droplet and the surface was relatively wide, corresponding to the pillar height. Finally, as shown in Fig. 8(e), the shape of the bottom part changed from a cylindrical shape into a conical frustum.

Fig. 8(c) shows the shape of the DCE droplets at the pillar height of 16.96 Å when the solid-surface characteristic energy was 1.0 kcal/mol. When the pillar height increased further, the

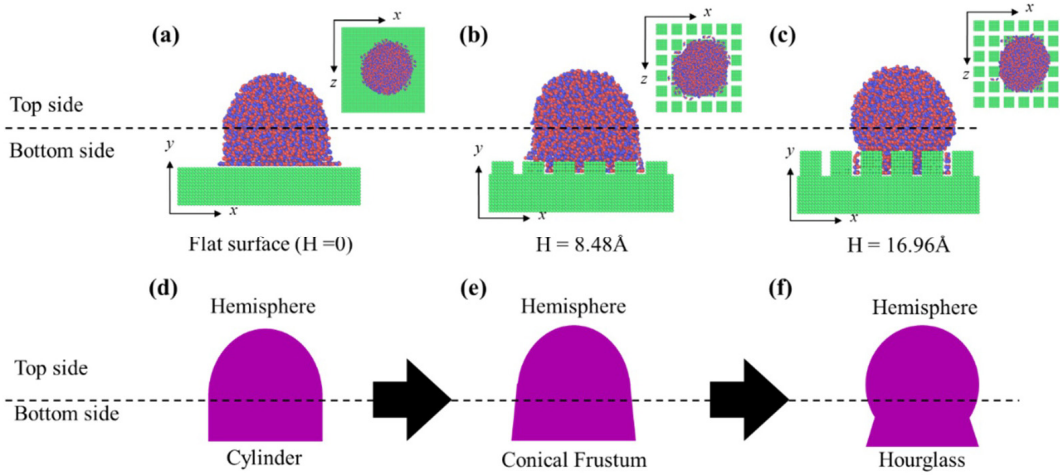

Fig. 8. Snapshots of DCE droplets corresponding to the pillar height of (a) 0; (b) 2.12 Å; (c) 16.96 Å, and their schematics for pillar heights of (d) 0; (e) 2.12 Å; (f) 16.96 Å, at the solid surface characteristic energy of 1.0 kcal/mol.

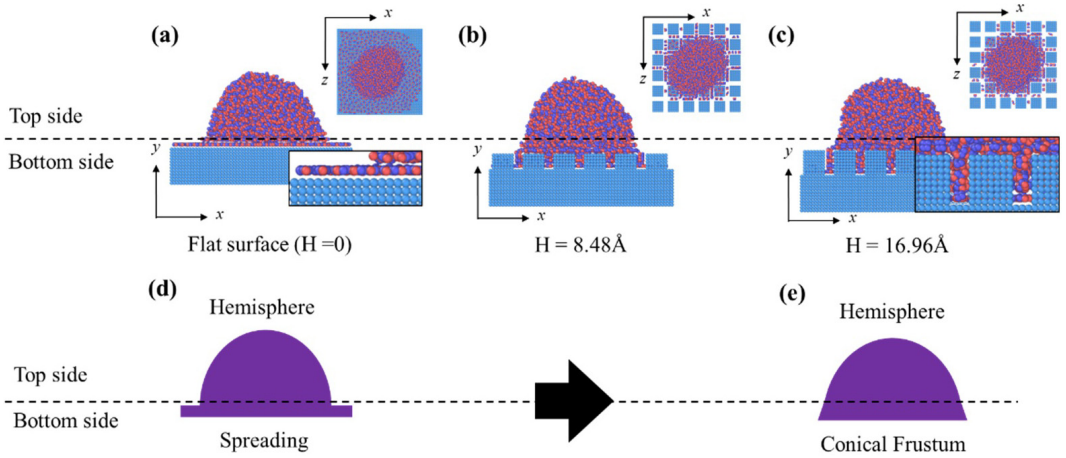

Fig. 9. Snapshots of DCE droplets corresponding to the pillar height of (a) 0; (b) 8.48 Å; (c) 16.96 Å, and their schematics for pillar heights of (d) 0; (e) 16.96 Å, at the solid surface characteristic energy of 20.0 kcal/mol.

distance between the DCE droplet and the flat plate increased, which weakened the influence of the flat plate on the top part of the DCE droplet. The bottom part of the DCE droplet concurrently interacted with the pillar and flat plate, causing only the bottom part of the DCE droplet to permeate the gaps due to the interaction with the surface. Consequently, the DCE droplet appeared to separate into two parts in terms of its shape. The top part of the DCE droplet still maintained its shape as a hemisphere, whereas the bottom part of the DCE droplet took on an hourglass shape, as shown in Fig. 8(f).

Fig. 9 shows snapshots of the water and oil droplets at various pillar heights under lipophilic conditions, along with schematic diagrams of the oil droplets.

Figs. 9(a)-(c) show snapshots of the DCE droplets at different pillar heights, corresponding to a solid-surface characteristic energy of 20.0 kcal/mol. Due to the strong attraction of the lipophilic pillars and the plate, the DCE droplet adopted a hemispherical shape. Interestingly, the DCE droplet exhibited spreading patterns on the surface, corresponding to the pillar height. On a flat lipophilic surface, the DCE droplet formed a hemispherical shape, but DCE molecules near the flat plate spread widely to create a coating-like layer, as shown in Fig. 9(a). As the pillar height increased from 0 to 8.48 Å, the DCE molecules permeated the gaps between the pillars, decreasing the spreading range. Finally, at a pillar height of 16.96 Å, the DCE molecules at the bottom of the droplet filled the gaps between the pillars, further decreasing the spreading range.

Figs. 9(d) and (e) show schematic diagrams of the DCE droplets on a lipophilic surface with a solid characteristic energy of 20.0 kcal/mol. Similar to the DCE droplet's shape on a weak lipophobic surface, the DCE droplet's shape on the lipophilic surface could be considered as two parts: the top and bottom parts. Irrespective of the pillar height, the top part of the droplet maintained its shape as a hemisphere, as shown in Figs. 9(d) and (e). Contrarily, the bottom part of the droplet changed depending on the pillar height. On a flat surface, the bottom part of the droplet spread and formed a layered shape, as shown in Fig. 9(d). As the pillar height increased, however,

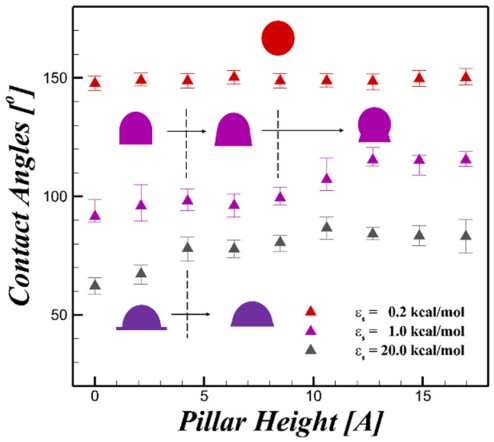

Fig. 10. Contact angles of DCE droplets corresponding to the pillar height and schematics for the DCE droplets' shapes.

the DCE molecules permeated the gaps of the pillars, and the bottom part of the droplet transformed into a conical frustum, as illustrated in Fig. 9(e). Furthermore, the spreading range decreased as the pillar height increased.

Fig. 10 shows the contact angles of the DCE droplets corresponding to pillar heights on various surfaces, accompanied by schematic representations of changes in DCE droplet shapes. The symbols in red, purple, and gray correspond to solid-surface characteristic energies ε_s of 0.2, 1.0, and 20.0 kcal/mol, respectively. Similarly, the schematics in red, purple, and dark purple represent solid-surface characteristic energies ε_s of 0.2, 1.0, and 20.0 kcal/mol, respectively.

As explained in Fig. 7, at the solid-characteristic energy of 0.2 kcal/mol, the contact angle and the shape of DCE droplet maintains as the pillar height increased. On the other hands, at the solid-characteristic energy of 1.0 and 20.0 kcal/mol, the contact angle of the DCE droplet significantly related with the pillar height.

At the solid characteristic energy of 1.0 kcal/mol, the contact angle of DCE droplet slightly increased from 91.70° to 96.10° and 98.75° as the pillar height increased from 0, 2.12 Å, and 4.24 Å. At 6.36 Å and 8.48 Å, the bottom part of the DCE droplet transformed into a conical frustum, and the contact angles were 97.94° and 99.25°, respectively, with a smaller change in contact angle compared with that at 4.24 Å. As the pillar height increased further to 10.6 Å and 12.72 Å, the bottom part of the DCE droplet adopted an hourglass shape, whereas the top part remained hemispherical, resulting in contact angles of 107.11° and 115.57°, respectively. The pillar height higher than 8.48 Å, which seems the depth of a potential bridge, significantly changed the contact angle and shape of the DCE droplet. At pillar heights higher than 12.72 Å, the contact angle converged to a value near 115°, similar to the converged contact angle of a water droplet at a solid-surface characteristic energy of 0.2 kcal/mol. Therefore, on the weak lipophobic surface, the variation in the contact angle of the DCE droplet was slight at low pillar heights but increased as the pillar height exceeded 8.48 Å.

For the lipophilic surface, whose solid-surface characteristic energy was 20.0 kcal/mol, the contact angle increased from 62.31° to 67.07° and 77.9° as the pillar height increased from 0 to 2.12 Å and 4.24 Å, respectively. The low-height pillars attracted the DCE molecules permeating the gaps between the pillars. Then, the bottom part of the DCE droplet transformed from a layer into a convex, increasing the contact angle. After transforming its shape, the contact angle remained almost constant about 82.63 ± 4.20°, with relatively small changes corresponding to the pillar height. The DCE molecules gathered around the DCE droplet and did not spread at these pillar heights. Thus, the DCE droplet maintained its shape as a hemisphere on a conical frustum, as shown in Figs. 9(c) and (e).

4. Conclusions

This study conducted molecular dynamics simulations to compare the behavior of water and oil droplets on the same surface, as well as to investigate the behavior of oil droplets on various surface conditions. In summary, the results demonstrated that, similar to water droplets, the behavior of oil droplets is significantly influenced by surface characteristics, including hydrophobicity, as well as surface geometry, particularly the presence of pillars and their height. However, it was observed that the behavior of oil droplets differs depending on the specific part within the droplet, in contrast to water droplets.

Under conditions with consistent solid-surface characteristic energy, it was observed that as the pillar height increased, the water droplet exhibited an increasing hydrophobic tendency, while the behavior of the oil droplet (DCE) remained largely consistent.

On weak lipophobic surfaces, the DCE droplet exhibited distinct behaviors in its top and bottom parts. The top part of droplet maintained a hemispherical shape, while the bottom part underwent a transformation from a cylindrical shape to a conical frustum, ultimately resembling an hourglass with increasing pillar height. Under lipophilic conditions, oil droplets exhibited permeation into the spaces between pillars due to strong interactions with surface atoms. Similar to DCE droplets on weak lipophobic surfaces, the top and bottom parts showed different shapes. While the top part of the droplet remains its hemispherical shape with increasing pillar height, the DCE molecules at the bottom, which initially spread on the surface and formed a coating-like layer, aggregate within the droplet. This aggregation leads to an increase in the contact angle of the DCE droplet, eventually converging to a specific value.

The implications of these findings extend to potential applications in the precise control of droplet behavior on surfaces, facilitating the separation and merging of diverse liquid types. By crafting structures with specific surface characteristics and morphologies, it becomes feasible to manipulate droplet behavior without the need for additional external forces or energy inputs. This research yields valuable insights for the design of surfaces with tailored wettability properties, thereby advancing

fields such as microfluidics, coatings, and biomedical devices.

Acknowledgments

This research was supported by the National Research Foundation of Korea (NRF) grant funded by the Korea government (MSIT) (NRF-2019R1A5A8083201). This research was supported by Basic Science Research Program through the National Research Foundation of Korea (NRF) funded by the Ministry of Education (RS-2023-00239843).

Nomenclature

A_n : Dihedral coefficient
H : Pillar height
K_{angle} : Angle constant
K_{bond} : Bond constant
q : Electric charge
r_{ij} : Distance between a pair of atoms i and j
U_{total} : Total potential between atom and molecules
U_{bond} : Potential by bonding
U_{angle} : Potential by bending
$U_{dihedral}$: Potential by torsion
$U_{coulomb}$: Coulomb potential
U_{LJ} : Lennard-Jones potential
ε_{ij} : Characteristic energy between a pair of atoms i and j
σ_{ij} : Characteristic length between a pair of atoms i and j
θ : Angle between three atoms
γ_{LG} : Surface tension of the liquid

References

[1] G. D. Bixler and B. Bhushan, Rice- and butterfly-wing effect inspired self-cleaning and low drag micro/nanopatterned surfaces in water, oil, and air flow, *Nanoscale*, 6 (2014) 76-96.
[2] S. H. Lim, Development of nanostructured superhydrophobic surfaces, *KIC News*, 15 (2012) 11-22.
[3] M. S. Ambrosia, M. Y. Ha and S. Balachandar, The effect of pillar surface fraction and pillar height on contact angles using molecular dynamics, *Applied Surface Science*, 282 (2013) 211-216.
[4] B. Xu, C. Zhang, Z. Chen, Y. Yang and Q. Cao, Investigation of nano-droplet wetting states on array micro-structured surfaces with different gravity, *Computers and Fluids*, 222 (2021) 104936.
[5] M. S. Ambrosia and M. Y. Ha, A molecular dynamics study of Wenzel state water droplets on anisotropic surfaces, *Computers and Fluids*, 163 (2018) 1-6.
[6] T. Mouterde, G. Lehoucq, S. Xavier, A. Checco, C. T. Black, A. Rahman, T. Midavaine, C. Clanet and D. Quere, Antifogging abilities of model nanotextures, *Nature Materials*, 16 (2017) 658-663.
[7] D. Ji, G. Liu, X. Zhang, C. Zhang and S. Yuan, Molecular dynamics study on the adsorption on heavy oil drops on a silica surface with different hydrophobicity, *Energy and Fuels*, 34 (2020) 7019-7028.
[8] L. Guo, G. Tang and S. Kumar, Droplet morphology and mobility on lubricant-impregnated surfaces: A molecular dynamics study, *Langmuir*, 35 (2019) 16377-16387.
[9] J. Gao, X. Yao, Y. Zhao and L. Jiang, Lyophilic nonwettable surface based on an oil/water/air/solid four-phase system, *Small*, 9 (2013) 2515-2519.
[10] S. Xu, J. Wang, J. Wu, Q. Liu, C. Sun and B. Bai, Oil contact angles in a water-decane-silicon dioxide system: effects of surface change, *Nanoscale Research Letters*, 13 (2018) 108.
[11] W. Wei, T. Zhou, L. Zhao, L. Deng and M. Xie, A Molecular Dynamics Investigation on fuel vaporization and mixing characteristics under Sub/supercritical conditions, *Thermal Science*, 26 (2022) 3517-3527.
[12] X. Li, D. Wang and T. Saeed, Multi-scale numerical approach to the polymer filling process in the weld line region, *Facta Universitatis-Series Mechanical Engineering*, 20 (2) (2022) 363-380.
[13] A. P. Thompson, H. M. Aktulga, R. Berger, D. S. Bolintineanu, W. M. Brown, P. S. Crozier, P. J. in 't Veld, A. Kohlmeyer, S. G. Moore, T. D. Nguyen, R. Shan, M. J. Stevens, J. Tranchida and S. J. Plimpton, LAMMPS–A flexible simulation tool for particle-based materials modeling at the atomic, meso, and continuum scales, *Computer Physics Communications*, 271 (2022) 10817.
[14] J. Delhommelle and P. Millie, Inadequacy of the Lorentz–Berthelot combining rules for accurate predictions of equilibrium properties by molecular simulation, *Molecular Physics*, 99 (2001) 619-625.
[15] D. J. Price and C. L. Brooks, A modified TIP3P water potential for simulation with Ewald summation, *The Journal of Chemical Physics*, 121 (2004) 10096-10103.
[16] H. Dong, Y. Zhou, C. Zheng and J. Zhou, On the role of the amphiphobic surface properties in droplet wetting behaviors via molecular dynamics simulation, *Applied Surface Science*, 544 (2021) 148916.
[17] J. P. Ryckaert, G. Ciccotti and H. J. C. Berendsen, Numerical integration of the cartesian equations of motion of a system with constraints: molecular dynamics of n-alkanes, *Journal of Computational Physics*, 22 (1977) 327-341.
[18] W. Shinoda, M. Shiga and M. Mikami, Rapid estimation of elastic constants by molecular dynamics simulation under constant stress, *Physical Review. Part B*, 69 (2004) 134103.
[19] G. J. Martyna, D. J. Tobias and M. L. Klein, Constant pressure molecular dynamics algorithms, *The Journal of Chemical Physics*, 101 (1994) 4177-4189.
[20] M. Parrinello and A. Rahman, Polymorphic transitions in single crystals: a new molecular dynamics method, *Journal of Applied Physics*, 52 (1981) 7182-7190.
[21] M. E. Tuckerman, J. Alejandre, R. Lopez-Rendon, A. L. Jochim and G. J. Martyna, A Liouville-operator derived measure-preserving integrator for molecular dynamics simulations in the isothermal–isobaric ensemble, *Journal of Physics A*, 39 (2006) 5629-5651.
[22] T. W. Kwon, K. H. Lee, Y. M. Seo, J. Jang and M. Y. Ha,

Dynamics wetting behaviors of water droplets on surfaces with dual structures at the nanoscale, *International Journal of Multiphase Flow*, 129 (2020) 103352.
[23] P. Liu and J. He, Geometric potential: An explanation of nanofiber's wettability, *Thermal Science*, 22 (2018) 33-38.
[24] N. Peng and J. He, Insight into the wetting property of a nanofiber membrane by the geometrical potential, *Recent Patents on Nanotechnology*, 14 (2020) 64-70.

Yun Ji Kang received her M.S. degree from Pusan National University, South Korea in 2023. Her research interests are focused on molecular dynamics and computational fluid dynamics.

Man Yeong Ha received his B.S. degree from Pusan National University, Korea, in 1981, M.S. degree, in 1983, from Korea Advanced Institute of Science and Technology, Korea, and Ph.D. degree from Pennsylvania State University, USA in 1990. Dr. Ha is currently a Professor at the School of Mechanical Engineering at Pusan National University in Busan, Korea. He served as an Editor of the Journal of Mechanical Science and Technology. He is the member of Honorary Editorial Advisory Board of the International Journal of Heat and Mass Transfer. His research interests are focused on thermal management, computational fluid dynamics, and micro/nano fluidics.